This is to certify that the
thesis entitled

COMPUTATIONAL FLUID DYNAMICS SIMULATION
OF A PULSED-JET MIXER

presented by

Dina Arafa Eldin

has been accepted towards fulfillment
of the requirements for the

Master's degree in Chemical Engineering

Charles A. Petty
Major Professor's Signature

August 21, 2003
Date

PLACE IN RETURN BOX to remove this checkout from your record.
TO AVOID FINES return on or before date due.
MAY BE RECALLED with earlier due date if requested.

DATE DUE	DATE DUE	DATE DUE

COMPUTATIONAL FLUID DYNAMICS SIMULATION OF A PULSED-JET MIXER

By

Dina Arafa Eldin

A THESIS

Submitted to
Michigan State University
in partial fulfillment of the requirements
for the degree of

MASTER OF SCIENCE

Department of Chemical Engineering and Materials Science

2003

ABSTRACT

COMPUTATIONAL FLUID DYNAMICS SIMULATION OF A PULSED-JET MIXER

By

Dina Arafa Eldin

The Hanford Site in southeastern Washington State contains 177 underground storage tanks that contain 53 million gallons of radioactive waste. One third of these tanks have already leaked and others are showing signs of wear. The Columbia River, which is just seven miles away from the site, is threatened by radioactive contamination. The radioactive waste in the tanks has settled into layers of liquid and sludge. The first challenge that arises is pumping the slurry, sludge and liquid mixture from the underground storage tanks. The second challenge is making sure the sludge does not settle within the pretreatment vessels. The proposed solution is to use a pulsed-jet mixer (PJM) to suspend the solid phase (sludge) in the liquid phase.

In this study, a commercial computational fluid dynamic code (FLUENT 6.0) is used to simulate the axisymmetric flow field induced by a pulsed-jet mixer symmetrically situated in a large tank. The simulation uses the volume-of-fluid multiphase model with a k-ε closure for the Reynolds stress. A discrete phase model is used to track the trajectories of individual solid particle in the JPM and the tank. Under the standard operating conditions of the PJM, The simulations shows that the pulsed-jet mixer under standard operating conditions could suspend heavy particles (specific gravity of 3) as large as 100 μm. However, 500 μm. particles settled to the bottom of the tank and are unable to be resuspended.

To my family

ACKNOWLEDGEMENTS

I would like to thank Dr. Charles Petty for his guidance during my undergraduate research work and graduate research, as well as the great impact to my academic and professional career.

I would also like to thank my family, for their continuous support, I could not have done this without them.

This research was supported by two grants from the National Science Foundation (NSF/EEC 9980325 and NSF/CTS 0083227). Thanks to the many people I have worked with on this project and previous NSF/CRCD projects. I have had the opportunity to work with a great group of mentors, Dr. Andre Benard, Dr. Steven Parks, Dr. Charles Petty, and Dr. Mei Zhuang.

Special thanks to Dr. Brigette Rosendall, who motivated the study of this problem, served as my industrial mentor, and allowed me the opportunity to work on the problem at Bechtel as a co-op student.

Thank you to my research group for all the help you have given me. I would especially like to thank a dear friend to me that always supported me, Munif Farhan. Special thanks to my friends I made during my graduate work at MSU.

TABLE OF CONTENTS

LIST OF TABLES

LIST OF FIGURES

LIST OF NOTATION

English Symbols

$C_{1\varepsilon}$	Model constant for *k*-ε turbulence model
$C_{1\varepsilon}$	Model constant for *k*-ε turbulence model
g	Gravity
k	Turbulent kinetic energy
P	Pressure
$\underline{\underline{S}}$	Rate of strain tensor
$\underline{u}$	Mass average velocity

Greek Symbols

α_1	Volume fraction of air
α_2	Volume fraction of water
ε	Turbulent dissipation
$\langle\mu\rangle$	Reynolds average of the mixture viscosity
μ_1	Viscosity of air
μ_2	Viscosity of water
μ_ε	Eddy viscosity
$\langle\rho\rangle$	Reynolds average of the mixture density
ρ_1	Density of air
ρ_2	Density of water
σ_k	Model constant for *k*-ε turbulence model
σ_ε	Model constant for *k*-ε turbulence model

CHAPTER 1

BACKGROUND

1.1 Hanford Site Background

The U. S. Department of Energy (DOE) Hanford Site, a 560 square-mile area in southeastern Washington State, has 177 large storage tanks containing radioactive waste. The tanks are seven miles south of the Columbia River, the largest river in the Pacific Northwest. Some of these tanks have leaked about one million gallons (two percent of the current waste volume) to the soil. Tank leakage has impacted the groundwater, and radionuclides are moving faster and deeper into the ground than previously estimated. Risks to the environment and the people living in the area will increase dramatically as more radionuclides reach the ground water.

The tank waste, which has been accumulating since 1944, is the result of producing plutonium for national defense during World War II and the Cold War. Approximately 53 million gallons of radioactive waste (sixty percent of the nation's waste) is stored in these aging tanks. Each tank contains between 50,000 to 1,000,000 gallons of waste. The storage tanks are divided into 149 old single-shell tanks and 28 new double-shell tanks. The single-shell tanks are 50 years old, on average, and 30 years beyond their design life. The double-shell tanks are quickly nearing their capacity. A temporary solution to the problem has been to replace the leaking single-shell tanks with the double-shell tanks.

A permanent solution is presently underway to clean all the tanks. The world's largest and most complex waste treatment facility is being built at the Hanford Site to immobilize the waste. This project will take ten years and four billion dollars to accomplish this task. The construction of the plant started in 2002 and will become operational in 2007. The plant will convert the waste into stable glass by a process called vitrification.

Vitrification is a proven technology used in the United States and Europe to immobilize radioactive waste in a stable form of glass to isolate it from the environment. Before the waste can be sent to the vitrification pre-treatment plant, the liquid and sludge in an underground storage tank must be mixed to form a slurry that can be mobilized (pumped). After the waste is mixed, the slurry will be pumped from the underground storage tank and sent to a pre-treatment plant. Once the slurry reaches the pre-treatment plant, mixing vessels are also used to ensure that the sludge remains suspended. The radioactive waste is separated into high- and low-radioactive sludge. The low activity waste is placed in canisters and buried in cement-lined trenches on site.

The high-activity waste is vitrified on site by mixing it with silica and other glass-making constituents. The mixture is heated to nearly 2000 °F in an electric smelter. The molten glass is poured into large stainless steel canisters and cooled for a few days. The canisters will be stored on the Hanford Site until they are shipped to a federal facility for permanent disposal.

1.2 Pulsed- Jet Mixer

Pulsed-jet mixers (PJMs) are a proven cost-effective technology for suspending concentrated sludge material in very large tanks (see Powell,1996; Daymo, 1997). The main advantage for using PJM technology over normal jet mixers is that they have few moving parts inside the tank. Furthermore, the parts that are inside the tank are less likely to malfunction than the components outside the tank. Thus, repairs can be made easily and safely outside the tank, which is obviously important if the material is radioactive. However, because PJMs are not as powerful as standard jet mixers, multiple mixers are needed for very large tanks.

The PJM has a frustoconical effluent nozzle that is close to the bottom of the tank (see Figure 1 and Table 1). A vacuum is created within the cylindrical chamber of the PJM to draw a relatively small amount of the suspension into the cylindrical chamber of the PJM. Once full, the pressure in the PJM is reversed and the fluid is discharged at a high velocity back into the tank. The repeated action of the PJM mobilizes the radioactive sludge near the bottom of the tank by creating a large-scale toroidal recirculation flow within the tank.

1.3 Objectives

In this thesis, computational fluid dynamics (CFD) is used to study the mixing performance of a pulsed-jet mixer (Patwardham,2001; Eldein, *et al.*, 2002). CFD provides a means for an early evaluation of design options. This is an important advantage for this problem because the fluid and the solid material are radioactive. Thus, CFD information can be used to support the testing program by identifying worthy designs and operating strategies. FLUENT 6.0, which uses a finite volume method to discritize the governing transport equations, was employed in this study.

The flow field in the jet and the tank is examined to learn about the fluid mechanics of the system. Before particles are injected into the flow field, the number of cycles for the velocity profile in the tank to reach a periodic solution is determined. Monitors in the computation domain are used to track the velocity as a function of time at different locations in the flow filed. Particle trajectory calculations are used to quantify the behavior of discrete particles in the spatially nonuniform and temporally unsteady, albeit periodic, flow field.

Studying the flow patterns and particle trajectories with CFD can provide new insights related to the potential for particle abrasion on solid surfaces. Stagnation zones in the flow field can be identified and areas of particle settlement ascertained. Thus, the results can assist in designing a tank/PJM design that minimizes the separation of solids. The CFD quantities of interest include the velocity magnitude, the velocity vectors, and the particle trajectories.

1.4 Methodology and Scope

The tanks in the pretreatment plant have round bottoms and may contain several PJMs and internal piping. In this study, a single PJM will be evaluated in a tank with no internal piping or surfaces other than the PJM itself. The 2D simulation developed in this study is axisymmetric and unsteady. The operation of the PJM is similar to the operation of an industrial PJM. For example, the suction phase is three times as long as the drive phase and the percentage of fluid within the jet canister at the start and end of the drive phase is the same as the industrial design (95% full at the onset and 8% full at end of the discharge cycle).

A VOF model supported by a k-ε closure for the Reynolds stress was used to track the air-liquid interface and to simulate the flow field within the PJM and tank. The following physical properties were used in the study:

liquid phase density: 998 kg/m^3
liquid phase viscosity: 0.001003 kg/m^2s
air phase density: 1.225 kg/m^3
air phase viscosity: 0.000017894 kg/m^2s
solid phase density: 3000 kg/m^3

The top of the tank is modeled as a free surface. The velocity at control surface S1 (see Figure 1) is calculated based on the required time for the drive phase (2 seconds) and the suction phase (6 seconds). A constant pressure of 0 Pa is set at control surface S2 (Figure 1).

An unsteady state Lagrangian particle trajectory calculation is used to determine the motion of the solid spherical particles. The particles are placed in the flow domain at various elevations within the tank (axial direction) and spaced equally over the horizontal plane (radial direction). The particle diameters encountered in practice range from 1μm to 600 μm. It is assumed that if a 100 μm particle stays suspended, then all particles smaller than 100 μm will also stay suspended. The 500 μm size was chosen to show how the system would handle the larger diameter particles. The particles were introduced with an initial velocity of zero.

1.5 Tables and Figures

Table 1 Dimensionless Parameters

D_T	0.91 m
D_J/D_T	0.28 m
H/D_T	1.41 m
H_1/D_N	0.46 m
H_2/D_T	variable
D_N/D_J	0.40 m
H_N/D_J	0.69 m

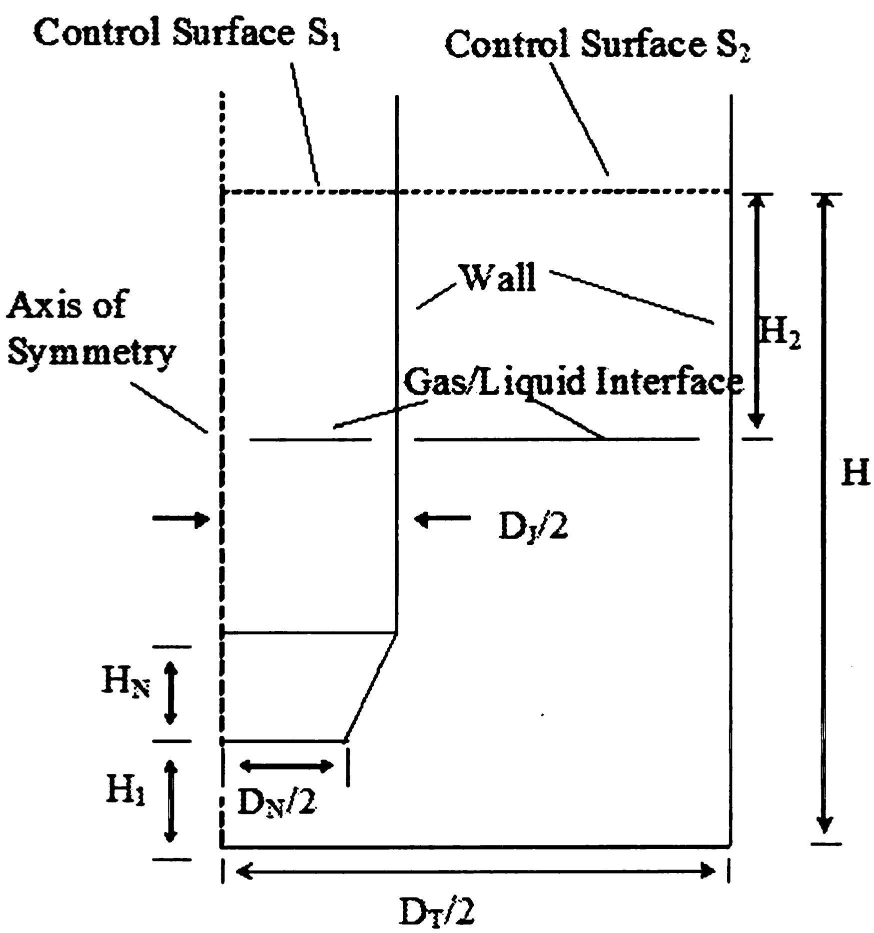

Figure 1 Geometry of Pulsed-Jet Mixer and Tank

CHAPTER 2

COMPUTATIONAL FLUID DYNAMICS MODEL

2.1 Volume of Fluid Model

The multiphase model used in this study is the VOF model supported by FLUENT 6.0 (see FLUENT, 2001; Hirt, 1981). The VOF model can be used for the transient tracking of two immiscible fluids. In this simulation, air is chosen as the primary phase and water as the secondary phase. This decision is based on identifying the primary phase as the material for which the boundary conditions are set (see FLUENT tutorial, 2001). The VOF model assumes that the divergence of the mean velocity field (i.e., the ensemble average of the mass weighted velocity of the two phases) is zero:

$$\nabla \cdot <\underline{u}> = 0 . \tag{1}$$

The VOF model also assumes that no mass transfer occurs between the two immiscible phases (air and water in this thesis). The tracking of the interface is accomplished by solving the continuity equation for the volume fraction of the secondary phase (water). Eq. (2) is the mean field continuity equation for the volume fraction of water:

$$\frac{\partial <\alpha_2>}{\partial t} + <\underline{u}> \cdot \nabla <\alpha_2> = 0 , \tag{2}$$

where α_2 is the volume fraction of water. The volume fraction α_1 of the primary phase (air) is determined from the constraint,

$$<\alpha_1> + <\alpha_2> = 1 . \tag{3}$$

The VOF model assumes that there is only one momentum equation shared between the two phases. Eq. (4) below is the turbulent version of the momentum equation,

$$\frac{\partial}{\partial t}(<\rho><\underline{u}>)+\nabla\cdot(<\rho><\underline{u}><\underline{u}>)=$$
$$-\nabla<P>+<\rho>\underline{g}+\nabla\cdot(2<\mu><\underline{\underline{S}}>-<\rho><\underline{u'u'}>) \tag{4}$$

In the above equation, $<\rho>$ is the volume-fraction-averaged density; $<P>$ is the pressure; g is the gravity; $<\underline{\underline{S}}>$ is the rate of strain tensor; and, $-<\rho><\underline{u'u'}>$ is the Reynolds stress. The Boussinesq hypothesis is used to model the Reynolds stress, as follows:

$$-\rho<\underline{u'}\ \underline{u'}>=$$
$$2\mu_e<\underline{\underline{S}}>-\frac{2}{3}<\rho>k\ \underline{\underline{I}} \tag{5}$$

In the above equation, μ_e represents an eddy viscosity and k is the turbulent kinetic energy. The momentum equation for the mixture is dependent on the volume fraction through the physical properties of the two phases:

$$<\rho>\equiv<\alpha_1>\rho_1+<\alpha_2>\rho_2 \tag{6}$$

where ρ_1 is the density of air and ρ_2 is the density of water. Also,

$$<\mu>\equiv<\alpha_1>\mu_1+<\alpha_2>\mu_2 \tag{7}$$

where μ_1 is the viscosity of air and μ_2 is the viscosity of water.

The turbulence model for the Reynolds stress in this simulation is the standard k-ε model (see FLUENT, 2001; Pope, 2000). The standard k-ε model is based on transport equations for the turbulent kinetic energy k and the dissipation ε:

$$\frac{\partial(<\rho>k)}{\partial t}+\nabla\cdot(<\rho>k<\underline{u}>) =$$

$$\nabla\cdot[(<\mu>+\frac{\mu_e}{\sigma_k})\nabla k]-<\rho><\underline{u}'\ \underline{u}'>:\nabla<\underline{u}>-<\rho>\varepsilon \tag{8}$$

$$\frac{\partial(<\rho>\varepsilon)}{\partial t}+\nabla\cdot(<\rho>\varepsilon<\underline{u}>)=$$

$$\nabla\cdot[(<\mu>+\frac{\mu_e^m}{\sigma_\varepsilon})\nabla\varepsilon\ ]-C_{1\varepsilon}<\rho><\underline{u'u'}>:\nabla<\underline{u}>]+\frac{\varepsilon}{k}-C_{2\varepsilon}<\rho>\frac{\varepsilon^2}{k} \tag{9}$$

where $\sigma_k = 1.0$; $\sigma_\varepsilon = 1.3$; $C_{1\varepsilon} = 1.44$; $C_{2\varepsilon} = 1.92$. A standard wall function is used near fluid/solid interfaces (see FLUENT, 2001).

2.2 Discrete Phase Model

The discrete phase model (Lagrangian equation of motion for solid particles) is used to determine the trajectories of individual solid particles in the flow field. The influence of turbulence on the dispersion of particles is neglected in this study. The trajectory calculations are based on a force balance on individual particles, using the local continuous phase conditions as the particle moves through the unsteady flow field. Particle position is updated as the solution advances in time. This uncoupled approach is used when the continuous phase flow pattern is not impacted by the discrete phase (i.e., dilute suspensions). Clearly, the discrete phase depends on the local hydrodynamic conditions of the continuous phase. In the uncoupled approach, the particle position and the flow field are both updated at the end of each time step.

The trajectory of a discrete phase particle is predicted by integrating the force balance on the particle. This force balance equates the particle inertia with forces acting on the particle as illustrated by Eq.(10) below:

$$\frac{\partial < \underline{u}_P >}{\partial t}\bigg|_{<X_p>} = F_D + \frac{\rho_P - < \rho >}{\rho_P}\underline{g}\,. \tag{10}$$

In the above equation, F_D is the drag per unit particle mass and depends on the slip velocity and the Reynolds number:

$$F_D = \frac{18 < \mu > C_D\,Re}{\rho_P d_p^2\, 24}(< \underline{u} > - \underline{u}_p)\,. \tag{11}$$

$<\underline{u}>$ is the fluid velocity of the suspension and $\underline{u}_p$ is the particle velocity. The mean viscosity and mean density of the fluid mixture are represented as $<\mu>$ and $<\rho>$, respectively. ρ_p is the density of an individual particle whereas the diameter of the particle is d_P. Re is the particle Reynolds number, which is defined as

$$Re = \frac{< \rho > d_p \left| < \underline{u} > - \underline{u}_p \right|}{< \mu >}\,. \tag{12}$$

The drag coefficient, C_D, is defined as follows (see FLUENT, 2001):

$$C_D = \frac{24}{Re}(1 + 0.1862\,Re^{0.6529}) + \frac{0.4373\,Re}{7174.584 + Re}\,. \tag{13}$$

The trajectory of an individual particle is calculated by integrating the following equation:

$$\frac{d < \underline{X}_P >}{d\,t} = < \underline{u}_P >\,. \tag{14}$$

2.3 Boundary Conditions

The PJM is situated on the axis of the cylindrical tank (see Figure 1). The simulation assumes that the unsteady flow field is axisymmetric with a plane of symmetry containing the axis of the tank and, thereby, the PJM. Therefore, only half of the geometry needs to be created in GAMBIT 2.0.

No-slip boundary conditions are imposed on all solid/fluid interfaces (i.e., tank walls, tank bottom, and PJM walls). A velocity inlet boundary was specified at a control surface located at the top of the jet-mixer and a pressure outlet boundary was specified at the control surface at the top of the tank (see Figure 1).

The mean velocity on the "inlet boundary" during the drive phase was 0.4803 m/s. The mean velocity on the "inlet boundary" during the suction phase was –0.1601 m/s, which is 1/3 of the magnitude of the drive velocity. The flow field was initialized from the values at the inlet (see Table 2).

The boundary condition on the solid particles included reflection at a solid/fluid interface and escape at the inlet and outlet boundaries. The solid particles were introduced at various locations in the flow domain (see Chapter 3) with a zero velocity.

2.4 Computational Domain

The tank is modeled as a flat bottom cylinder with an inner diameter of 0.91 m and a height of 1.29 m (see Figure 1 and Table 1). The cylindrical part of the mixer has a height of 1.07 m and an inner diameter of 0.25 m. A conical nozzle, which has a contraction ratio of 2.5:1, is attached to the bottom of the cylinder. The end of the nozzle is 0.048 m above the bottom of the tank. The length of the pulsed-jet mixer is 1.24 m.

In the simulation, the tank and the pulsed-jet mixer are open at the top. The control surface within the jet is at the same height as the control surface of the tank. Under quiescent conditions (i.e., no flow), the liquid phase occupies 95% of the jet volume. At the end of the drive phase of the cycle, the liquid phase occupies 8% of the jet volume, which is about the volume of the nozzle.

The geometry is discritized into computational cells, which are also known as control volumes. In this geometry, a non-uniform grid was used inasmuch as a finer grid is needed near fluid/solid interfaces due to the no slip boundary condition. Also, an unstructured grid was employed for the nozzle portion of the geometry, and the triangular part of the flow domain adjacent to the nozzle (see Figure 2 and Figure 3). The number of computational cells used in the simulation is 13, 894. The grid was fine enough to allow for a grid independent solution, but course enough to yield a converged result in a reasonable amount of time.

2.5 Tables and Figures

Table 2 Initial Conditions

Gauge Pressure (pascal)	0
Axial Velocity (m/s)	0.4803
Radial Velocity (m/s)	0
Turbulence Kinetic Energy (m^2/s^2)	0.000473718
Turbulence Dissipation Rate (m^2/s^3)	9.52862e-5
Water Volume Fraction	0

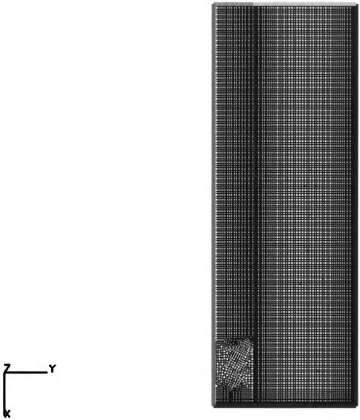

Figure 2 Computational Fluid Dynamics Grid

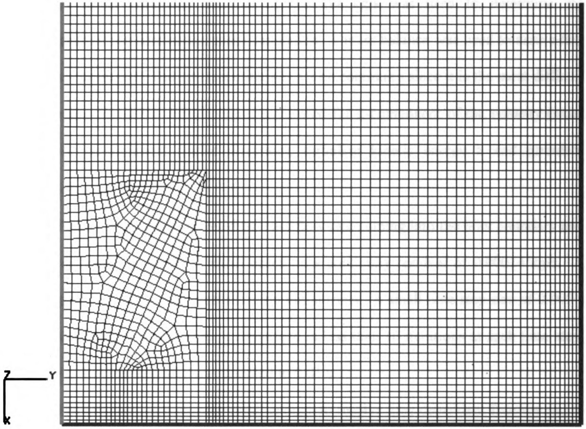

Figure 3 Computational Fluid Dynamics Grid (continued)

CHAPTER 3

RESULTS

3.1 Numerical Results

A target continuity residual of 0.00014 kg/s was used to determine the convergence of the continuous phase simulation. A mass balance was used to assure that mass was conserved. The strictest criteria is set on continuity since it is the most difficult to converge. FLUENT default values were used for x-component of the velocity (axial direction), y-component (radial direction), turbulent kinetic energy k and turbulent dissipation ε.

Table 3 shows that the residual mass flow rate coming into the inlet boundary and leaving the outlet boundary is small based on a continuity residual of 0.00014 kg/s. A time step size of 0.01 s was used based on initial trials. A small time step size of 0.005 s was initially used and the solution converged in less than 10 iterations at each time step. Therefore, the time step size was doubled to 0.01 s.

The time step size must be small enough to resolve time dependent features and to ensure convergence within 20 iterations. The simulation was set to make 20 iterations per time step, but the solution would converge within 15 iterations at the beginning of the drive phase or suction phase. The number of iterations to reach convergence continued to decrease till it reached 2 iterations at the end of the drive or suction phase. With this step size, 200 time steps were needed to simulate the 2 s drive phase and 600 time steps were needed for the 6 s suction phase. It took approximately 1 hour of real time to simulate the drive phase and 3 hours of real time to simulate the suction phase.

3.2 Fluid Dynamic Results

Due to the importance of color in understanding the results, **images in this thesis are presented in color.**

The magnitude of the velocity on the control surface S1 (see Figure 1) during the drive phase and the suction phase of the cycle is shown in Figure 4. The entire cycle is 8 s (2 s drive phase and 6 s suction phase). The five lines struck in Figure 4 mark the times in the cycle when subsequent simulation results will be shown. Time "a" corresponds to 0.0001 s into the drive phase; time "b" corresponds to 1 s. The drive phase is stopped a time "c" (= 2 s) and the suction phase is started. Time "d" corresponds to 3 s into the suction phase and time "e" (= 8 s) is at the end of the suction phase and the beginning of the drive phase. The reason for showing the results at 0.0001 s is due to the fact that 0 s is the end of Cycle 2. A time step with a size of 0.0001 s is used to show the results at the beginning of Cycle 3.

The transient to a periodic state occurs rapidly. Cycle 3 essentially reproduces itself at larger times. A periodic solution in the velocity profile was observed to occur during Cycle 2. The magnitude of the velocity within the PJM was monitored at six spatial locations. Figures 5 and 6 show the results for three cycles. The spatial coordinates of each monitor are defined on the figures. The results clearly demonstrate that a periodic solution is attained within three cycles.

Figures 7-11 show the instantaneous flow field for Cycle 3 at the five different times defined by Figure 4 (i.e., "a"-"e"). A white line is used to mark the air-water interface. The air is the red portion above the interface. The boundaries of the PJM are outlined with a black line. The green line is the surface used to specify the drive and suction velocities. And the blue line is the outlet pressure boundary. The calculation is an axisymmetric calculation, but is mirrored for clarity along the axis of symmetry. The axisymmetric boundary condition was specified at the red vertical line.

Figure 7 shows the velocity magnitude and vectors at the start (0.0001 s) of drive phase in Cycle 3. The fluid coming outside the nozzle cause a recirculation pattern that takes up approximately 50% of the water volume in the annular region. In the annular region, the velocity is still relatively low, due to the low velocity during the suction phase. The recirculation zone is circulating in an inward motion towards the jet. The streamlines of the fluid not participating in the circulating region are moving upward. The highest velocity is at the inside part of the nozzle. In the lower part of the jet there is a stagnant region due to switching from the drive phase to the suction phase. Also, in this stagnant region, it can be seen that some of the vectors are still pointing upward and have not switched direction.

Figure 8 shows the velocity magnitude and vectors at the middle (1 s) of the drive phase in Cycle 3. It can be seen that the interface has moved halfway down the jet and slightly higher in the annular region. The overall size of the recirculation zone remains the same, but the center of the recirculation zone has moved to the corner of the tank. Due to the high velocity coming form the nozzle, the bottom of the tank and the bottom quarter of the side wall of the tank has a higher velocity than the beginning of the drive phase. The velocity in the cylindrical part of the jet is constant; the high velocity at the nozzle now extends to the entire exit area of the nozzle.

Figure 9 shows the velocity magnitude at the end of the drive phase in Cycle 3. It can be seen that the interface has moved down the cylindrical part of the jet toward the effluent nozzle while the interface in the annular region has moved up. Although the overall size of the recirculation zone remains the same, the center of the recirculation zone has clearly moved up relative to Figure 8. In the annular region there are high regions of velocity due to the recirculation zone moving at a high velocity. The high velocity issuing form the nozzle also causes high velocities in the bottom third of the tank. The high velocity region extending to the side of the wall has increased in Figure 9 compared with Figure 8. The velocity in the jet remains constant except near the interface. The velocity contours in the nozzle region are about the same in Figures 8 and 9.

Figure 10 shows the velocity magnitude at the middle (5 s) of the suction phase in Cycle 3. It can be seen that the interface has moved back to the same location as the middle of the drive phase. The overall size of the recirculation zone is larger than during the drive phase, approximately two-thirds of the flow field participates in the recirculating region. The center of the recirculation zone has moved slightly upward and away from the side wall. The vectors in the top third of the annular region are pointed in the downward direction. The high velocity at the bottom of the tank and side walls has vanished. The velocity profile in the nozzle region of the jet resembles a flame, and contains a recirculation zone near the angled part of the nozzle. This recirculation pattern did not exist during the drive phase, but it can be seen at 0.0001 s that the recirculation in the corner moves out towards the axis of symmetry, and has vanished at 1 s.

Figure 11 shows the velocity magnitude at the end of the drive, which corresponds to the end of Cycle 3. The interface has moved back to the same location as the beginning of the drive phase. The overall size and location of the recirculating region stays the same. The after effect from the drive phase of the high velocity in the recirculation zone has disappeared. The velocity profile in the jet remains the same. Due to the low velocity during the suction phase, significant changes in the flow field do not occur.

It is noteworthy that during the drive phase, a low velocity region (color coded green) surrounded by high velocity fluid (color coded red) develops near the bottom of the tank along the symmetry plane. This phenomena also occurs during the suction phase, but in this case the region is stagnant.

Two stagnation points develop during the cycle. The first exists during the drive phase, the second during the suction phase. The stagnation point during the drive phase is found at the bottom of the tank on the symmetry plane. It can be seen that the vectors in this region point towards the bottom of the tank and are unable to turn. During the suction phase the stagnation point has shifted. It occurs where the streamlines split the circulating region and flow returning to the nozzle of the jet.

FLUENT's user manual (see Section 27.4, FLUENT, 2001) defines the static pressure as a gauge pressure relative to a reference pressure (by default, 101,325 Pa). The absolute pressure, therefore, is the sum of the static pressure and the reference pressure. The gauge pressure on the control surface S2 is specified as 0 Pa during the drive phase, which implies that the absolute pressure on S2 is one atmosphere. Half way through the drive phase the pressure difference between control surface S1 (see Figure 1) and control surface S2 is 14, 435.41 Pa. Towards the end of the drive phase, the pressure difference increases to 19,397 Pa.

3.3 Lagrangian Particle Tracking Results

Forty particles are injected at the beginning of Cycle 3 and tracked for the entire cycle. Ten particles are injected at four different elevations in the tank, seven are in the annular region and three are in the jet region. Particles are placed between the nozzle and bottom of the tank, in the recirculation zone, directly above the recirculation zone and in the area where the bulk of the fluid does not enter the circulating region. Placing the particles at different starting position will help to determine how the starting position effects particle impingement and particle settlement.

The initial placement of the particles can be seen in Figure 12. The particles are color coded. The purple particles are placed 1.2622 m from the top of the tank, the blue particles are placed 0.9675 m from the top of the tank, the green particles are placed 0.6450 m from the top of the tank, and the red particles are placed 0.3325 m from the top of the tank. All the particles are equally distributed over the cross section (i.e., evenly spaced along the y-axis). The results of the trajectory calculations will be shown at the same times as the fluid dynamics results. These figures will also be mirrored along the axis of symmetry.

The first simulation is for particle having a diameter of 100 μm and a density of 3000 kg/m^3. The second simulation is for particles with the same density but a particle diameter of 500 μm. A comparison between the 100 μm and 500 μm particle results is given in Section 3.3.3 below.

3.3.1 100 μm case

The trajectory of the purple particles during the entire cycle will be discussed first. This discussion will be followed by observations related to the blue particle, the green particles, and the red particles.

At 1 s (see Figure 13), nine of the ten purple particles have moved into the center of the recirculation zone. The remaining purple particle is near the wall of the tank and is slightly higher than the rest of the particles. This is the particle that was initially closest to the wall of the tank. The vectors near the wall are pointing in an upward direction and cause the purple particle to move upward. At 2 s (see Figure 14), the nine purple particles are still in the recirculation zone and are following the center of the recirculating region. The remaining purple particle is further from the side wall and is following the streamlines and recirculating flow outside the group. At 5 s (see Figure 15), nine purple particles remain near the origin of the recirculation zone, while the remaining one is circulating in the outer region still. At 8 s (see Figure 16), nine purple particles are recirculating centrally; one purple particle remains circulating in the outside region.

The seven blue particles that were initially in the recirculating zone are located in a diagonal like fashion at 1 s (see Figure 13). The particle near the side wall of the tank is at the highest position and the one closest to the nozzle of the jet is at the lowest position. The three blue particles that were initially in the jet region have traveled across the bottom of the tank towards the side wall. The high velocity at the side of the wall pushes them up the wall. The one that is furthest along the side wall is the particle that started near the wall of the jet. The one that is close to the bottom corner of the tank is the particle that was initially near the symmetry plane. When the particles are initially injected, it is seen from the fluid mechanics that the region near the wall of the jet has a higher velocity relative to the stagnant region in the center. The stagnant region causes the particles near the symmetry plane to reach the side of the tank last. At 2 s (see Figure 14), six blue particles are at different elevations near the side of the wall, while the remaining four are in the circulating region. At 5 s (see Figure 15), the blue particles along the side wall are pushed into the recirculating region. A single blue particle remains in a stationary position. It is seen that two green particles and two red particles will join the blue particle in this location. At this position there is a balance in the force pushing the particle upward and the force pushing the particle downward. The velocity is high enough to keep pushing the particles up, but following the streamlines and curving is too difficult for these particles, in which gravity is pushing them down. At 8 s, Figure 16 shows that nine blue particles continue to circulate outside the purple particles and one of these blue particles circulates with a red particle. One still remains in the interesting stationary location with two green particles and two red particles. Since the velocity does not change much during the suction phase, it is expected that what is observed during the middle of the suction will also be observed at the end of the suction phase.

At 1 s into the drive phase, Figure 13 shows that four of the seven green particles will be caught in the recirculating region while the other three are moving upward toward the top of the tank. The green particles in the jet region follow the same trend as the blue particle in the jet region. The green particles near the jet wall furthest down the jet and the green particles near the symmetry plane are at the lowest position and are positioned in a diagonal like fashion. At 2 s, Figure 14 indicates that the three green particles came down the center traveled across the bottom of the tank and were pushed up the side wall.

The three green particles in the annular region are still approaching the top of the tank, while the other four are entering the recirculating zone. At 5 s, Figure 15 shows that the three green particles in the annular region are no longer traveling upward to the top of the tank inasmuch as the circulating region has captured the three green particles. Note that four green particles circulate outside the blue particles. Two are near the limiting streamline, but they spilt off in the region where they enter the recirculation zone and the jet. Two of the green particles are being swept back inside the jet. Two of the green particles are in the stationary position with the single blue particle and the two red particles. At 8 s, Figure 16 shows that the two green particles in the stationary location remain in the stationary location. Three of the green particles are traveling in an upward direction in the jet region. The other five green particles are recirculating around the blue particles. One of the green particles is coming down the limiting streamline.

Figure 13, which corresponds to 1 s into the drive phase, shows that seven of the ten red particles are moving upward toward the top of the tank. The three red particles in the jet region are moving down the jet all at the same elevation. At 2 s, Figure 14 shows that the three red particles are now in the corner of the tank; the other seven red particles are moving upward and are at a higher elevation than observed at 1 s. At 5 s, Figure 15 indicates that the seven red particles in the annular region are moving downward but remain in the flow field outside the recirculating zone. One of the red particles is in the recirculation region, while two are stuck in the stationary region with the other particles previously discussed. At 8 s, Figure 16 shows that the seven red particles in the annular region have moved down more, but not enough to enter the streamline of the circulating region. The two red particles in the stationary region remain at this location. The single circulating red particle is now circulating with one of the blue particles.

3.3.2 500 μm case

At 1 s, Figure 17 clearly shows that seven purple particles are in the corner of the tank, two are recirculating in the center, and one is recirculating a little higher and near the wall. At 2 s, Figure 18 indicates that seven purple particles remain in the corner, while the other three continue to recirculate (two near the center and the other one higher up in the flow field). At 5 s (see Figure 19) and at 8 s (see Figure 20), two purple particles continue to circulate and follow streamlines in the center, while the other particle is recirculating further out. The seven purple particles that quickly settled into the corner at 1 s are still in the corner and are unable to be resuspended during the entire cycle.

At 1 s, Figure 17 shows that three blue particles that were traveling down the jet are now in the corner of the tank. Six of the seven blue particles in the annular region are situated diagonally in the circulating region, while one is at the bottom of the tank. At 2 s (see Figure 18), five blue particles are circulating while five are in the corner of the tank. At 5 s (see Figure 19), only four blue particles continue to circulate, while the particles in the corner of the tank continue to accumulate. At 8 s (see Figure 20), only two blue particles are circulating.

The ten green particles at 1 s (Figure 17) are located as follows: three are coming down in the jet; two are at the bottom of the tank; and, the remaining single gree particle is at the exit of the nozzle. As indicated above, the last particle to reach the exit of the nozzle is the particle that started near the symmetry plane. The seven green particles in the annular region are split between two destinations; two green particles look like they will move up and five others look like they will move down. At 2 s (Figure 18), the three coming down the jet have moved to the corner of the tank. Seven are in the recirculation region, while a single green particle looks like it is moving upward. At 5 s (Figure 19), seven green particles are in the corner of the tank, one is circulating, one is traveling upward, and one is stuck in a stagnant region near the symmetry plane. At 8 s (Figure 20), one green particle is still traveling upward in the jet, eight are in the corner, and one is still in the stagnant region on the symmetry plane.

At 1 s into the drive phase, seven red particles in the annular region are moving down the tank against the streamlines, as indicated by Figure 17. The three red particles in the jet are moving downward in the jet. At 2 s (Figure 18), the particles in the jet are now in the corner, while the other seven have continued to move down. At 5 s (Figure 19), three red particles are still in the corner. The seven red particles that were in the annular region have now entered the recirculating zone. At 8 s (Figure 20), one of the 500 μm diameter red particles remains circulating, one is traveling upward in the jet, and the one particle that came down the limiting streamline is now in the stagnant region. Seven of the ten red particles remain in the corner.

During the suction phase, the magnitude of the velocity on control surface S1 is decreased. Therefore, the velocity vectors are no longer going straight at the wall. This causes the particles in the corner to move slightly out of the corner during the middle of the suction phase. Unfortunately, this movement away from the corner is not sufficient to resuspend the particles. Note that the particles have slide back into the corner even more during the end of suction. This movement may cause wear at bottom corner of the tank since the particles are being scraped back and forth between the drive and suction phase.

3.3.3 Comparison

In general, the 100 μm and 500 μm simulations showed similar trends. The 500 μm particles tended to settle faster, and were unable to be resuspended due to gravity and an adverse flow field.

At 1 s into Cycle 3 (drive phase), it is seen that all the particles are further along in the jet or annular region for the 500 μm case. The purple particles followed the same trend in which they stayed centralized in the recirculation zone, with one particle circulating outside them closer to the wall. For the 500 μm case, it is seen that seven of the purple particles already settled to the corner. The blue particles in both cases follow the diagonal distribution. The green particles also have the same distribution. Four of the 100 μm diameter particles are traveling to the top, while only three of the 500 μm particles are traveling to the top. The 100 μm red particles in the annular region are moving upward while the 500 μm red particles are moving down.

At 2 s, the purple particles are still following the same motion. In both cases, the 500 μm particles are circulating outside the purple particles. Also both cases have blue particles along the side wall. The green particles are also following the same trend. The 500 μm diameter particles were unable to travel along the wall and are stuck in the corner. In both cases, the tree red particles that traveled down the jet are now in the corner of the tank. It is noteworthy that the particles in the annular region are traveling in the direction of the streamlines in the 100 μm case, while in the 500 μm case they are crossing streamlines.

At 5 s (suction phase), the 100 μm and the 500 μm green particles circulate around the blue particles, and the blue particles circulate around the purple particles. In the 100 μm case, two particles are traveling in the jet, while in the 500 μm case only one particle is in the jet. One particle is stuck in the stagnant region. In the 500 μm case, the red particles in the annular have traveled downward and have entered the recirculation region.

At 8 s it is seen that more particles in the 500 μm case are in the corner of the tank and are unable to be resuspend. At the end of suction phase, the particles that are settled are still at the bottom of the tank. In the 100 μm case, the particles that reached the bottom of the tank or corner of the tank never were stuck, they could always be resuspended.

Two critical zones were found where particles might tend to drop from the recirculating region. In the drive phase, this is near the axis of symmetry when exiting the nozzle. In the suction phase, there is a limiting streamline between the recirculation zone and the fluid that is pulled back into the jet. If the particles follow this limiting streamline they may hit the bottom of the tank. The stationary location that was found during the suction phase for the 100 μm particle is not observed for the 500 μm case.

3.4 Tables and Figure

Table 3 Mass Balance

Time (s)	Inlet Mass Flow Rate (kg/s)	Outlet Mass Flow Rate (kg/s)	Difference
0.0001	-0.0099376747	0.0099106142	-2.7060509e-05
1	0.029813023	-0.029800106	1.2917444e-05
2	0.029813023	-0.029797886	1.5137717e-05
5	-0.0099376747	0.0099277413	-9.9334866e-06
8	-0.0099376747	0.0099234516	-1.4223158e-05

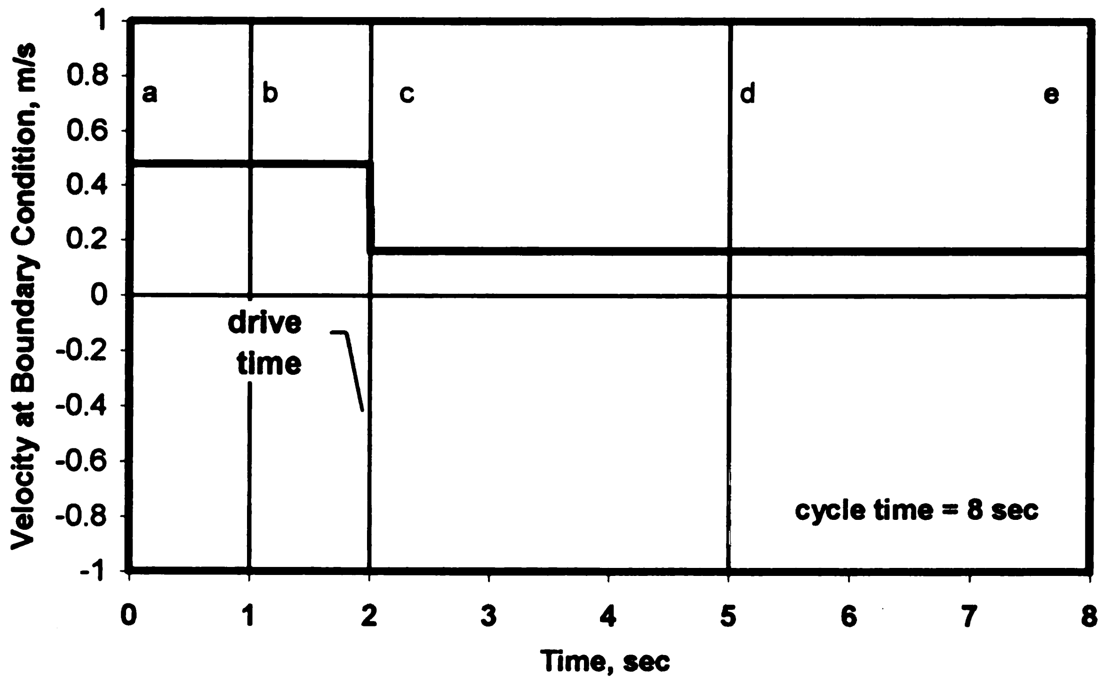

Figure 4. Velocity Profile

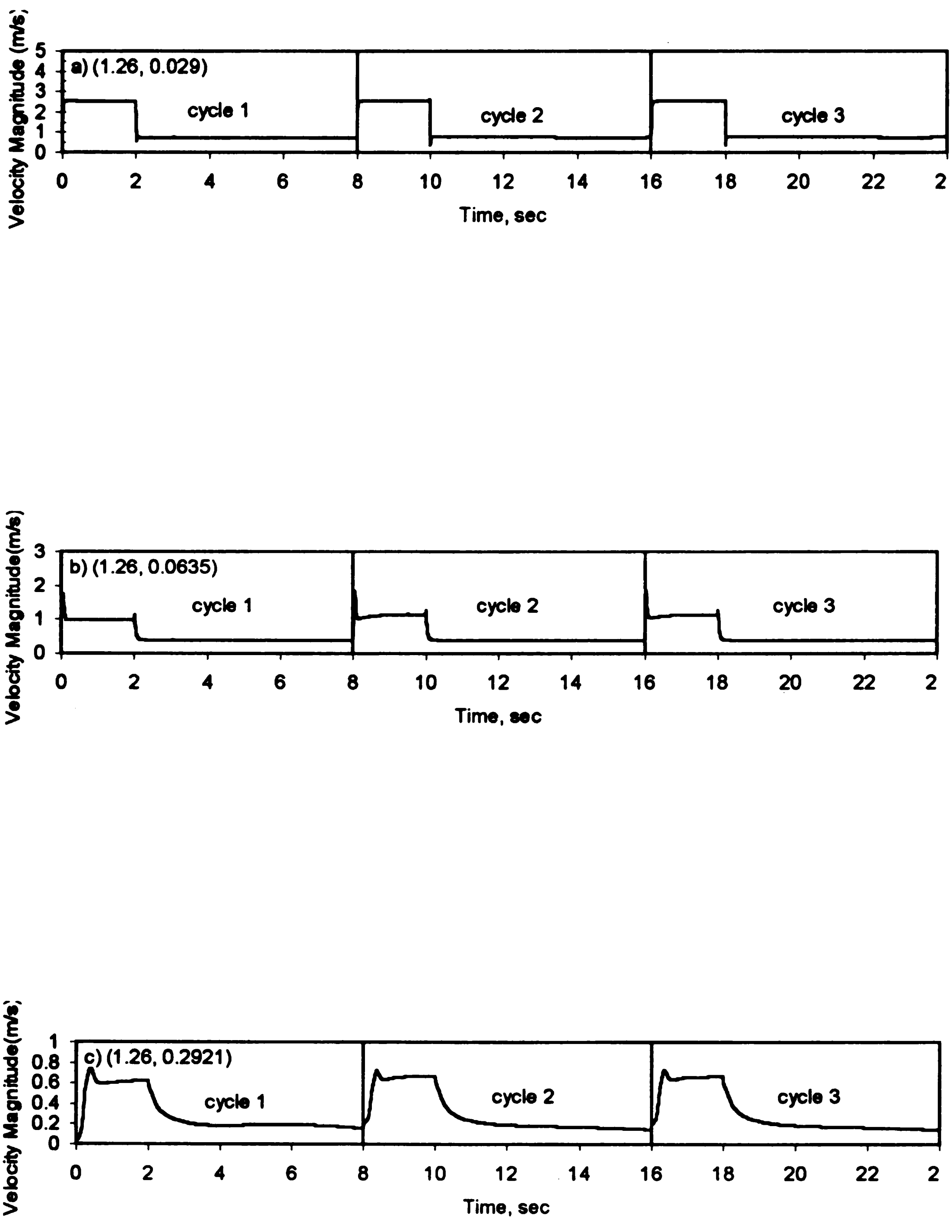

Figure 5 Velocity as a Function of Time

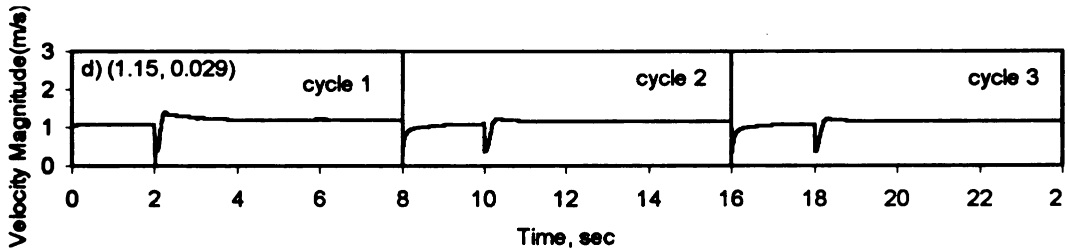

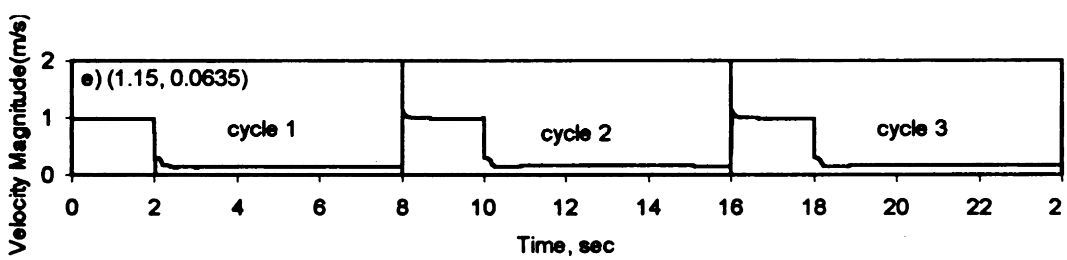

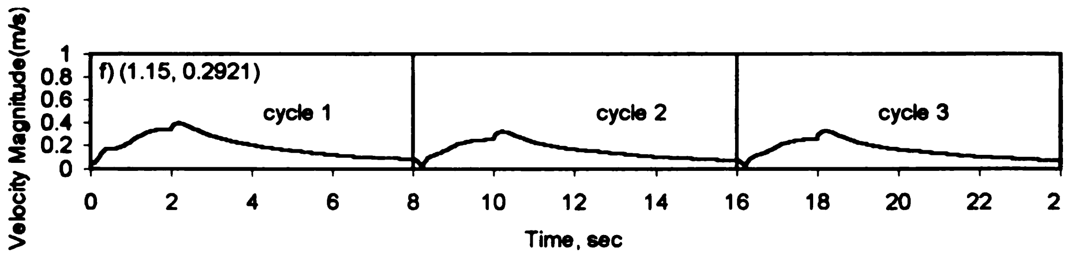

Figure 6 Velocity as a Function of Time (continued)

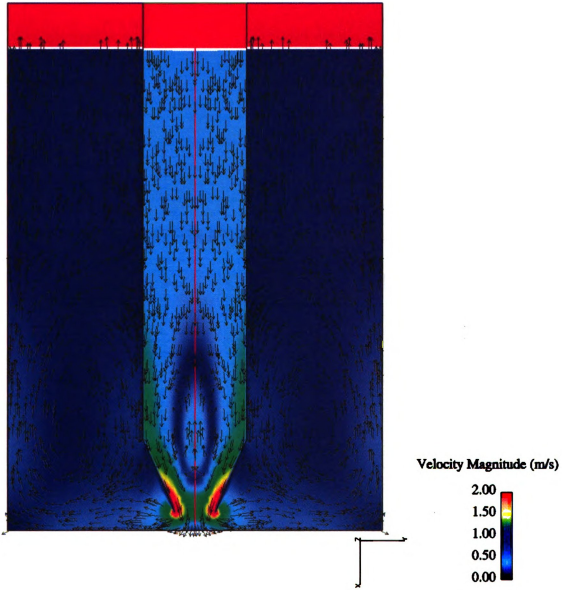

Figure 7 Contours of Velocity Magnitude and Velocity Vectors at the Beginning of Drive (0.0001 s), max velocity = 4.64 m/s

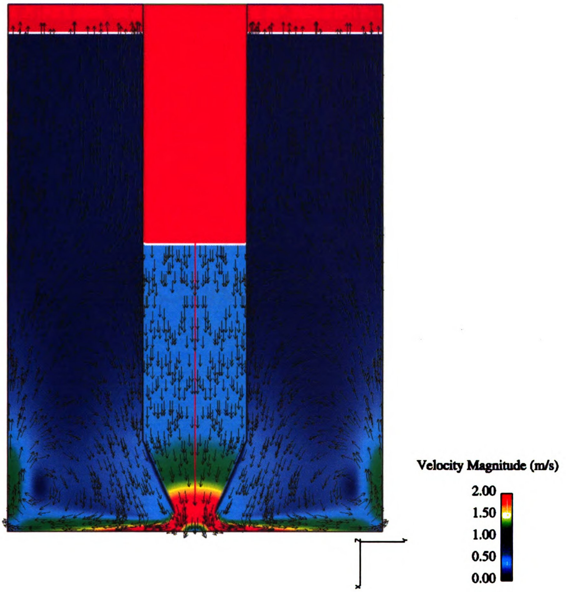

Figure 8 Contours of Velocity Magnitude and Velocity Vectors at the Middle of Drive (1 s), max velocity = 3.50 m/s

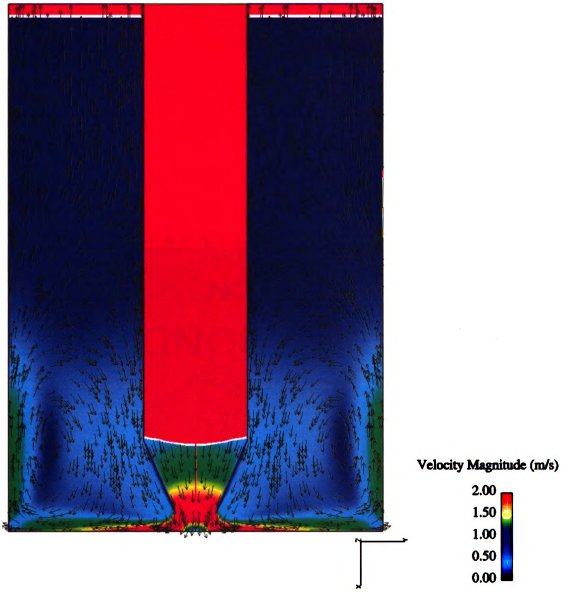

Figure 9 Contours of Velocity Magnitude and Velocity Vectors at the End of Drive (2 s), max velocity = 3.50 m/s

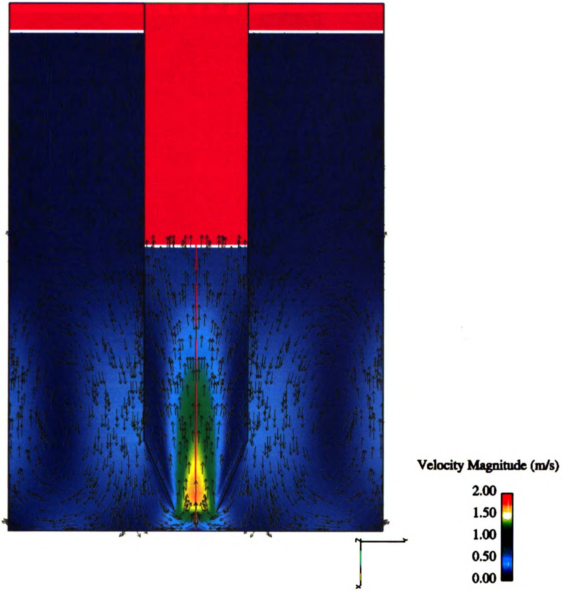

Figure 10 Contours of Velocity Magnitude and Velocity Vectors at the Middle of Suction (5 s), max velocity = 1.70 m/s

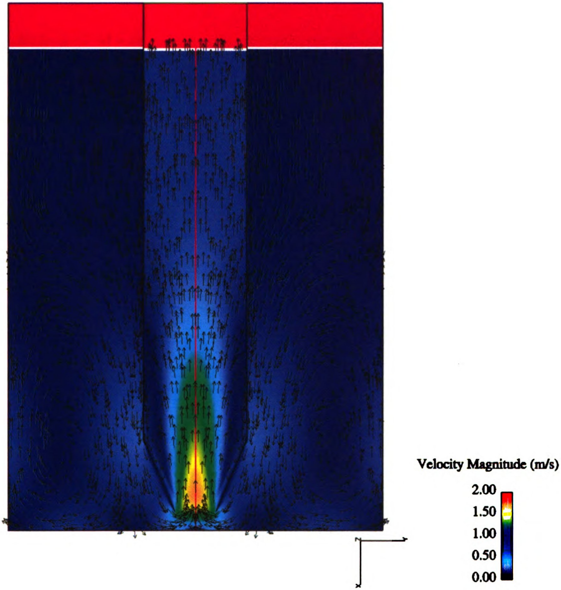

Figure 11 Contours of Velocity Magnitude and Velocity Vectors at the End of Suction (8 s), max velocity = 1.72 m/s

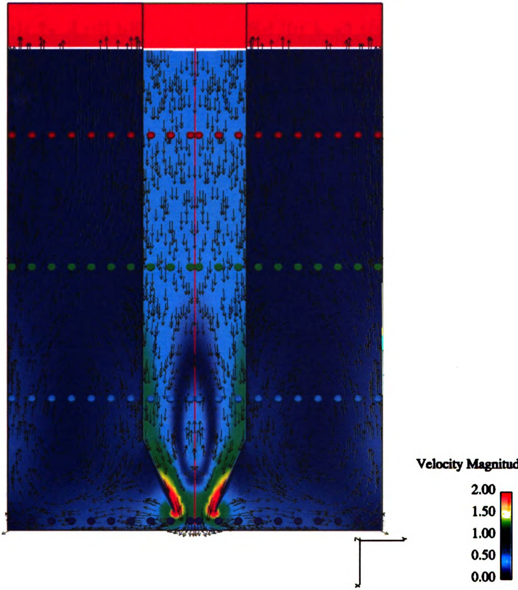

Figure 12 Initial Placement of Particles in Flow Field at Beginning of Drive (0.0001 s)

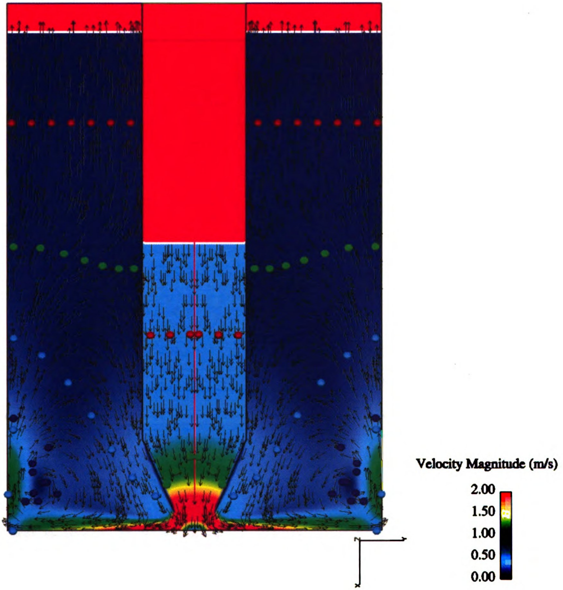

Figure 13 Particle Trajectories at Middle of Drive (1 s) for 100 μm Particle Diameter

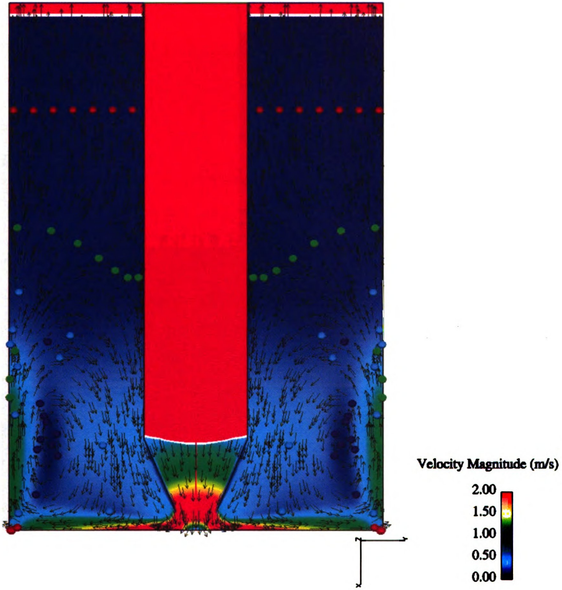

Figure 14 Particle Trajectories at End of Drive (2 s) for 100 μm Particle Diameter

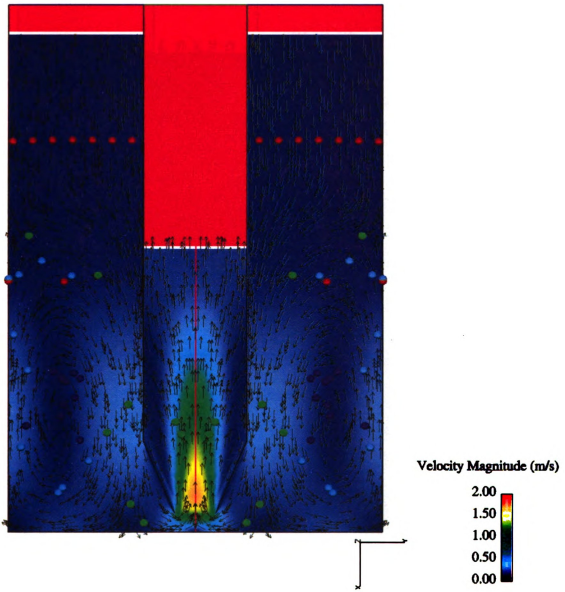

Figure 15 Particle Trajectories at Middle of Suction (5 s) for 100 μm Particle Diameter

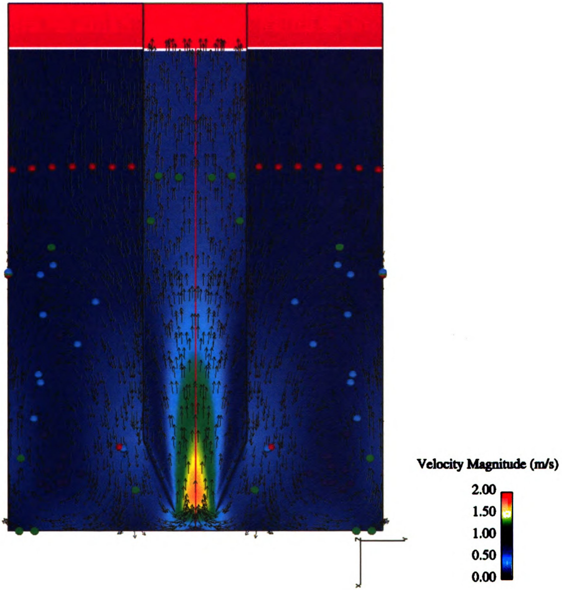

Figure 16 Particle Trajectories at End of Suction (8 s) for 100 μm Particle Diameter

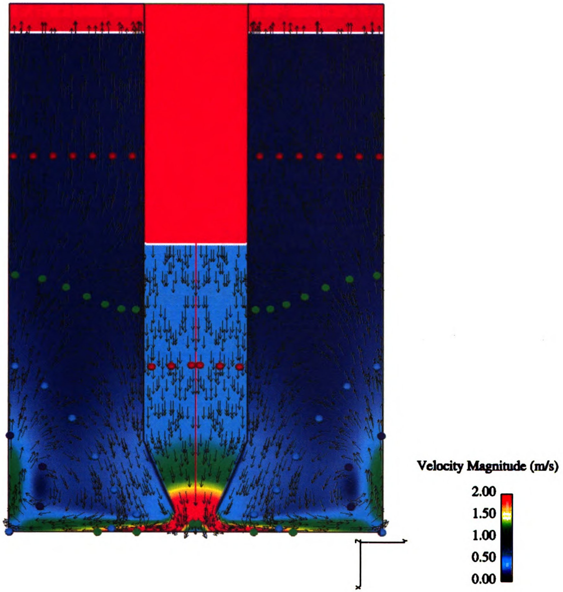

Figure 17 Particle Trajectories at Middle of Drive (1 s) for 500 μm Particle Diameter

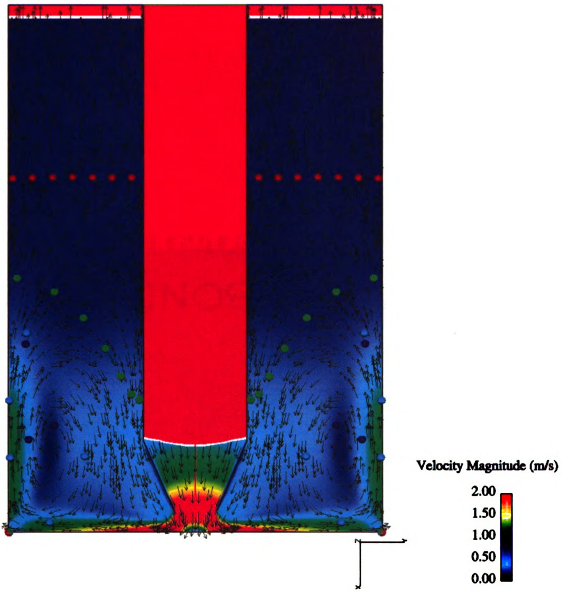

Figure 18 Particle Trajectories at End of Drive (2 s) for 500 μm Particle Diameter

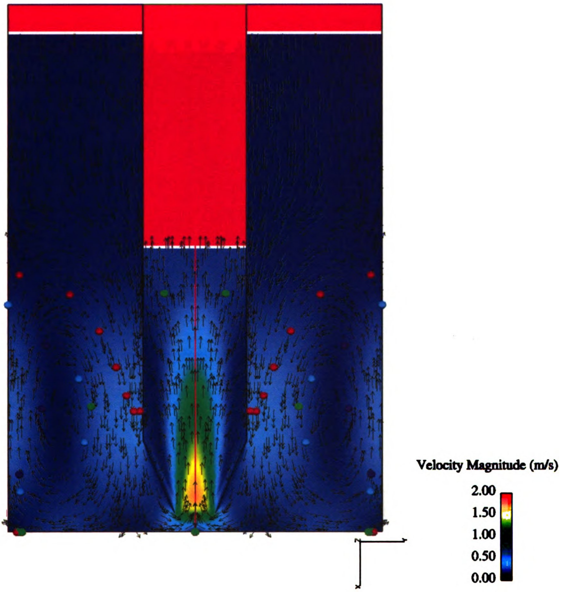

Figure 19 Particle Trajectories at Middle of Suction (5 s) for 500 μm Particle Diameter

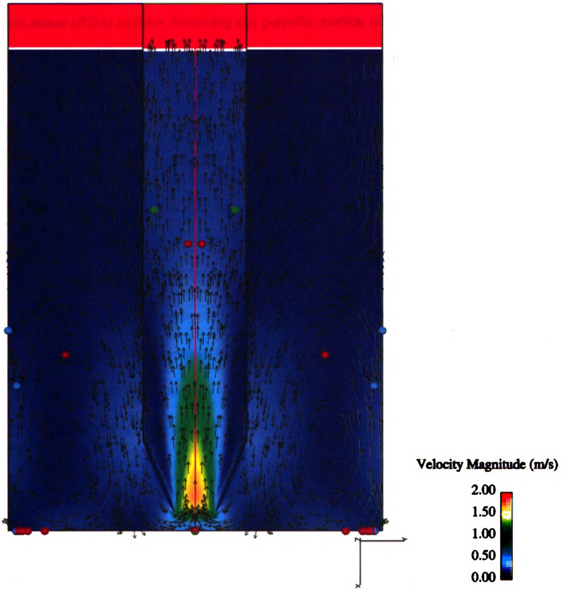

Figure 20 Particle Trajectories at End of Suction (8 s) for 500 μm Particle Diameter

CHAPTER 4

CONCLUSIONS AND RECOMMENDATIONS

4.1 Fluid Dynamics

The VOF model is an effective tool for tracking the moving interface of a pulsed-jet mixer (PJM) and for following the periodic motion of the flow field within the tank. Within two PJM cycles, the flow field exhibited a repetitive behavior. Two stagnation points were predicted, one during the drive phase and another during the suction phase. The size of the toroidal recirculation zone increases during the suction phase compared to the drive phase.

The high velocity at the nozzle exit during the drive phase may cause wear on the bottom of the tank due to particle impingement. A noteworthy result of this study is the prediction that a secondary flow develops within the nozzle during the suction phase of the cycle. This phenomenon could cause wear on the inside surface of the nozzle due to the repetitive abrasive action of the suspension at the fluid/solid interface.

4.2 Solid/Liquid Mixing

Under the conditions of this study (see Chapter 1), the large-scale toroidal recirculation zone within the tank does not cause particles with diameters less than 100 μm to migrate across streamlines; however, 500 μm diameter particles do cross streamlines by centrifugal action and gravity. Thus, a dilute dispersed phase having a particle size distribution with a maximum particle size less than 100 μm will remain suspended over a full cycle of the PJM. However, a PJM operating at a higher velocity is needed to keep 500 μm particles suspended.

Particles with diameters less than 100 μm on the bottom of the tank can be resuspended by the action of the recirculation zone. However, the recirculation flow cannot resuspend particles larger than 500 μm in diameter unless the jet velocity is increased significantly. After a few cycles, all of the large larger particles end up at the bottom of the tank near the outer wall.

The discrete particle study was helpful in determining the fate of particles over a single cycle of the PJM. Although most of the 500 μm diameter particles were separated from the suspension after multiple cycles, the ones that did stay suspended followed the same trends as the 100 μm particles. The following observations were deduced from the simulation (see Chapter 3 for definition of the color code used to define the initial position of a particle):

- purple particles are most likely to stay in the center of the re-circulation zone;
- blue particles stay in the re-circulating region, circulating around the purple particles and travel along the side of the wall;
- green particles are drawn into the recirculating region and circulate around the blue particles, but these particles are also likely to travel back into the jet region during the suction phase;
- green particles also travel up the wall whereas the red particles in the annular region will stay in the bulk of the flow field;
- with the exception of the 500 μm diameter particles, particles located in the annular region of the flow field do not enter the recirculating zone;
- 500 μm diameter particles located in the annular region travel towards the bottom of the tank and across streamlines.

As note above, the high velocity encountered at the nozzle exit during the drive phase may cause wear at the fluid/solid interface due to particle impingement. The tank bottom is especially vulnerable to this phenomenon. Furthermore, secondary flows that develop within the nozzle during the suction phase of the cycle could also cause significant wear due to the grinding action of the suspension at the fluid/solid interface. Surfaces on the outer wall of the tank may also be susceptible to wear due to the cyclical abrasive grinding motion of the suspension. Clearly, this CFD study has identified critical surfaces that may be more susceptible to wear than other more quiescent surfaces. PJM and tank design standards should address the possibility of toughening these critical surfaces.

4.3 Recommendations

Future CFD studies can include modifications to the geometry such as a round bottom tank, placing the nozzle at different heights from the bottom of the tank, and using different diameter nozzles. Angled firing from the jets can also be studied to see if this helps mitigate the potential of large particles accumulating in the corner of the tank. Also, studies can be done with more than one jet firing at a time. The synchronized action of multiple PJMs may improve the mixing action of this technology in unanticipated ways.

Different closure models for the Reynolds stress, for example the RSM model, can be used to simulate the turbulent transport phenomena in the tank and to assess the sensitivity of the results to this modeling assumption. Also, different multiphase models are available in FLUENT 6.0, such as the Mixture Model and the Eulerian Granular Model.

The flow within the tank and within the cylindrical jet could be uncoupled by setting a velocity boundary condition at the nozzle exit and setting a wall boundary condition at the top of the jet. This approach, which will disguise the secondary flows induced within the nozzle, would permit computational resources to be allocated to the flow domain within the tank. This would be important for a CFD study of more than one PJM in a single tank.

APPENDIX A : FLUENT MODEL SETUP

FLUENT
Version: axi, segregated, vof, ske, unsteady (axi, segregated, VOF, standard k-epsilon, unsteady)
Release: 6.1.18
Title:

Models

Model	Settings
Space	Axisymmetric
Time	Unsteady, 1st-Order Implicit
Viscous	Standard k-epsilon turbulence model
Wall Treatment	Standard Wall Functions
Heat Transfer	Disabled
Solidification and Melting	Disabled
Species Transport	Disabled
Coupled Dispersed Phase	Disabled
Pollutants	Disabled
Soot	Disabled

Boundary Conditions

Zones

name	id	type
fluid	2	fluid
wall-shadow	8	wall
wall	3	wall
axis	4	axis
wall	5	wall
outlet	6	pressure-outlet
inlet	7	velocity-inlet
default-interior	9	interior

Boundary Conditions

fluid

Condition	Value

Material Name	air
Specify source terms?	no
Source Terms	0
X-Velocity Of Zone	0
Y-Velocity Of Zone	0
Rotation speed	0
Deactivated Thread	no
Laminar zone?	no
Set Turbulent Viscosity to zero within laminar zone?	yes
Porous zone?	no
Porosity	1

wall-shadow

Condition	Value
Wall Motion	0
Shear Boundary Condition	0
Define wall motion relative to adjacent cell zone?	yes
Apply a rotational velocity to this wall?	no
Velocity Magnitude	0
X-Component of Wall Translation	1
Y-Component of Wall Translation	0
Define wall velocity components?	no
X-Component of Wall Translation	0
Y-Component of Wall Translation	0
Wall Roughness Height	0
Wall Roughness Constant	0.5
Discrete Phase BC Type	2
Normal	((polynomial angle 1))
Tangent	((polynomial angle 1))
Discrete Phase BC Function	none
Impact Angle Function	((polynomial angle 1))
Diameter Function	((polynomial 1))
Velocity Exponent Function	((polynomial 0))
Rotation Speed	0
X-component of shear stress	0
Y-component of shear stress	0

wall

Condition	Value
Wall Motion	0
Shear Boundary Condition	0
Define wall motion relative to adjacent cell zone?	yes

Apply a rotational velocity to this wall?	no
Velocity Magnitude	0
X-Component of Wall Translation	1
Y-Component of Wall Translation	0
Define wall velocity components?	no
X-Component of Wall Translation	0
Y-Component of Wall Translation	0
Wall Roughness Height	0
Wall Roughness Constant	0.5
Discrete Phase BC Type	2
Normal	((polynomial angle 1))
Tangent	((polynomial angle 1))
Discrete Phase BC Function	none
Impact Angle Function	((polynomial angle 1))
Diameter Function	((polynomial 1))
Velocity Exponent Function	((polynomial 0))
Rotation Speed	0
X-component of shear stress	0
Y-component of shear stress	0

axis

Condition Value

----

wall

Condition	Value
Wall Motion	0
Shear Boundary Condition	0
Define wall motion relative to adjacent cell zone?	yes
Apply a rotational velocity to this wall?	no
Velocity Magnitude	0
X-Component of Wall Translation	1
Y-Component of Wall Translation	0
Define wall velocity components?	no
X-Component of Wall Translation	0
Y-Component of Wall Translation	0
Wall Roughness Height	0
Wall Roughness Constant	0.5
Discrete Phase BC Type	2
Normal	((polynomial angle 1))
Tangent	((polynomial angle 1))
Discrete Phase BC Function	none
Impact Angle Function	((polynomial angle 1))

Diameter Function	((polynomial 1))
Velocity Exponent Function	((polynomial 0))
Rotation Speed	0
X-component of shear stress	0
Y-component of shear stress	0

outlet

Condition	Value
Gauge Pressure	0
Backflow Direction Specification Method	1
Axial-Component of Flow Direction	1
Radial-Component of Flow Direction	0
X-Component of Axis Direction	1
Y-Component of Axis Direction	0
Z-Component of Axis Direction	0
X-Coordinate of Axis Origin	0
Y-Coordinate of Axis Origin	0
Z-Coordinate of Axis Origin	0
Turbulence Specification Method	1
Backflow Turb. Kinetic Energy	1
Backflow Turb. Dissipation Rate	1
Backflow Turbulence Intensity	0.043199999
Backflow Turbulence Length Scale	0.061489001
Backflow Hydraulic Diameter	0.91439998
Backflow Turbulent Viscosity Ratio	10
Discrete Phase BC Type	4
Discrete Phase BC Function	none
is zone used in mixing-plane model?	no
Specify targeted mass-flow rate	no
Targeted mass-flow	1

inlet

Condition	Value
Velocity Specification Method	2
Reference Frame	0
Velocity Magnitude	0.4803
Axial-Velocity	0
Radial-Velocity	0
Axial-Component of Flow Direction	1
Radial-Component of Flow Direction	0
X-Component of Axis Direction	1
Y-Component of Axis Direction	0

Z-Component of Axis Direction	0
X-Coordinate of Axis Origin	0
Y-Coordinate of Axis Origin	0
Z-Coordinate of Axis Origin	0
Angular velocity	0
Turbulence Specification Method	1
Turb. Kinetic Energy	0.050000001
Turb. Dissipation Rate	0.25400001
Turbulence Intensity	0.036999999
Turbulence Length Scale	0.01778
Hydraulic Diameter	0.01778
Turbulent Viscosity Ratio	10
Discrete Phase BC Type	4
Discrete Phase BC Function	none
is zone used in mixing-plane model?	no

default-interior

Condition   Value

Solver Controls

Equations

Equation	Solved
Flow	yes
Volume Fraction	yes
Turbulence	yes

Numerics

Numeric	Enabled
Absolute Velocity Formulation	yes

Unsteady Calculation Parameters

Time Step (s)	0.001
Max. Iterations Per Time Step	20

Relaxation

Variable	Relaxation Factor
Pressure	1
Density	1
Body Forces	1
Momentum	0.7
Volume Fraction	0.6
Turbulence Kinetic Energy	0.7
Turbulence Dissipation Rate	0.7
Turbulent Viscosity	1

Linear Solver

Variable	Solver Type	Termination Criterion	Residual Reduction Tolerance
Pressure	V-Cycle		0.1
X-Momentum	Flexible	0.1	0.7
Y-Momentum	Flexible	0.1	0.7
Volume Fraction	Flexible	0.1	0.7
Turbulence Kinetic Energy	Flexible	0.1	0.7
Turbulence Dissipation Rate	Flexible	0.1	0.7

Discretization Scheme

Variable	Scheme
Pressure	Body Force Weighted
Pressure-Velocity Coupling	PISO
Momentum	First Order Upwind
Turbulence Kinetic Energy	First Order Upwind
Turbulence Dissipation Rate	First Order Upwind

Solution Limits

Quantity	Limit
Minimum Absolute Pressure	1
Maximum Absolute Pressure	5000000
Minimum Temperature	1
Maximum Temperature	5000
Minimum Turb. Kinetic Energy	1e-14
Minimum Turb. Dissipation Rate	1e-20
Maximum Turb. Viscosity Ratio	100000

Material Properties

Material: water-liquid (fluid)

Property	Units	Method	Value(s)
Density	kg/m3	constant	998.2
Cp (Specific Heat)	j/kg-k	constant	4182
Thermal Conductivity	w/m-k	constant	0.6
Viscosity	kg/m-s	constant	0.001003
Molecular Weight	kg/kgmol	constant	18.0152
L-J Characteristic Length	angstrom	constant	0
L-J Energy Parameter	k	constant	0
Thermal Expansion Coefficient	1/k	constant	0
Degrees of Freedom		constant	0

Material: air (fluid)

Property	Units	Method	Value(s)
Density	kg/m3	constant	1.225
Cp (Specific Heat)	j/kg-k	constant	1006.43
Thermal Conductivity	w/m-k	constant	0.0242
Viscosity	kg/m-s	constant	1.7894e-05
Molecular Weight	kg/kgmol	constant	28.966
L-J Characteristic Length	angstrom	constant	3.711
L-J Energy Parameter	k	constant	78.6
Thermal Expansion Coefficient	1/k	constant	0
Degrees of Freedom		constant	0

Material: steel (inert-particle)

Property	Units	Method	Value(s)
Density	kg/m3	constant	3000
Cp (Specific Heat)	j/kg-k	constant	502.48
Thermal Conductivity	w/m-k	constant	16.27

LIST OF REFERENCES

Daymo, E. A., 1997, "Industrial Mixing Techniques for Hanford Double-Shell Tanks", Pacific Northwest National Laboratory, PNNL-11725, UC-721.

Eldein, D.(presenter), S. Teich-McGoldrick, J. Roth, and C. Trainer, 2002, "CFD Simulation of a Pulsed-Jet Mixer", Undergraduate Poster Session, Annual AIChE Meeting, November 3-8, Indianapolis Convention Center, Indianapolis, Indiana.

FLUENT, 2001, User's Manual, FLUENT Inc., Lebanon, New Hampshire.

Hirt, C.W. and B.D. Nichols, 1981, "Volume of Fluid (VOF) Method for Dynamics of Free Boundaries", J. Comput. Physics, 39:210-225.

Patwardhan, A.W., 2001, **CFD Modeling of Jet Mixed Tanks**, Pergamon Press.

Perry, R.H., D. W. Green, and J.O. Maloney, 1984, **Perry's Chemical Engineering Handbook,** 6th Edition, McGraw-Hill Book Company.

Pope, S. B., 2000, **Turbulent Flows**, Cambridge University Press, Cambridge, UK.